Cobalt sulfide-reduced graphene oxide: An efficient catalyst for the degradation of rhodamine B and pentachlorophenol using peroxymonosulfate

Lylia Amirache, Fatiha Barka-Bouaifel, Priyakshree Borthakur, Manash R. Das, Hania Ahouari, Herve Vezin, Alexandre Barras, Baghdad Ouddane, Sabine Szunerits, Rabah Boukherroub

Version of Record: https://www.sciencedirect.com/science/article/pii/S2213343721009957
Manuscript_ab3a05ece011837b7714cab6bcd6f024

Cobalt sulphide-reduced graphene oxide: An efficient catalyst for the degradation of rhodamine B and pentachlorophenol using peroxymonosulfate

Lylia Amirache[1,2], Fatiha Barka-Bouaifel[2], Priyakshree Borthakur[3,4], Manash R. Das[3,4], Hania Ahouari[5,6], Hervé Vezin[5], Alexandre Barras[1], Baghdad Ouddane[5], Sabine Szunerits[1] and Rabah Boukherroub[1*]

[1]*Univ. Lille, CNRS, Centrale Lille, Univ. Polytechnique Hauts-de-France, UMR 8520 - IEMN, F-59000 Lille, France*

[2]*Laboratoire de Technologie des Matériaux et de Génie des Procédés (LTMGP), Faculté de Technologie - Université de Bejaia, 06000 Bejaia, Algérie*

[3]*Advanced Materials Group, Materials Sciences and Technology Division, CSIR-North East Institute of Science and Technology, Jorhat 785006, Assam, India*

[4]*Academy of Scientific and Innovative Research (AcSIR), CSIR-NEIST Campus, India*

[5]*Univ. Lille, UMR CNRS 8516- LASIRE Laboratoire Avancé de Spectroscopie pour les Intéractions la Réactivité et l'Environnement 59655 Villeneuve d'Ascq, France*

[6]*Univ. Lille, FR 2638 - IMEC – Institut Michel-Eugène Chevreul, F-59000 Lille, France*

*To whom correspondence should be addressed: Rabah Boukherroub, e-mail: rabah.boukherroub@univ-lille.fr; Tel: +333 62 53 17 24

Abstract

In this study, cobalt sulphide-reduced graphene oxide (CoS-rGO) nanocomposite was prepared by a solvothermal route and its structure, morphology and composition were assessed using various techniques, including transmission electron microscopy (TEM), Fourier transform infrared spectroscopy (FTIR), Raman spectroscopy, X-ray photoelectron spectroscopy (XPS) and thermogravimetric analysis (TGA). The catalytic performance of CoS-rGO was evaluated for activation of peroxymonosulfate (PMS) for the elimination of rhodamine B (RhB) and pentachlorophenol (PCP) in water. The effects of various operating parameters on the degradation efficiency were systematically studied. Under optimized operating conditions, the CoS-rGO/PMS system achieved fast (less than 10 min) elimination of RhB and PCP at room temperature, as evidenced by high-performance liquid chromatographic analysis (HPLC). Electron Paramagnetic Resonance (EPR) studies along with scavenging experiments revealed that sulphate radicals ($SO_4^{-\bullet}$) were the primary players in the catalytic process. Interestingly, the CoS-rGO catalyst was stable after 8 cycles without obvious activity loss. The results reported in the present study hold promise for potential application of CoS-rGO for PMS activation for the elimination of various organic pollutants.

Keywords: Cobalt sulphide; Reduced graphene oxide; PMS; Rhodamine B; Pentachlorophenol

1. Introduction

Water is a vital element for the survival of living beings. The contamination of water resources, due to the discharge of several organic pollutants from agricultural, urban and industrial activities, is a problem of world-wide scale that needs special attention. Most of these organic pollutants are harmful to eco-environment and human being, calling for their degradation/removal before being discharged into water. Among organic pollutants, rhodamine B (RhB) is an important synthetic dye used in the textile industry, owing to its good stability. However, RhB is potentially toxic, carcinogenic, and neurotoxic to humans and animals [1, 2]. Another persistent organic pollutant is pentachlorophenol (PCP). It is commonly applied as wood preservative, herbicide, and pesticide. It is characterized by high toxicity, carcinogenicity, and persistence [3-6]. PCP could be found in various environmental compartments, including air, water, land and aquatic sediments, soils… Therefore, RhB and PCP removal/degradation from wastewater effluents becomes nowadays a major topic of research.

The elimination of organic pollutants is particularly difficult, because they are persistent in the environment. Over the past decades, several techniques have been developed for organic pollutants removal from water using various approaches like adsorption, membrane separation, biological treatment, ion exchange, advanced oxidation processes (AOPs), and photocatalysis [7-15], etc. AOPs occupy a particular place among these techniques, owing to their efficacy to eliminate recalcitrant molecules under relatively mild conditions [14, 15].

The working principle of AOP is to produce very active species ($OH^{\bullet}$,$O_2^{-\bullet}$, $SO_4^{-\bullet}$) for the effective degradation and, in some cases, full mineralization of persistent organic molecules and pathogens in water [16]. Currently, the Fenton reagent is frequently used for the treatment of wastewater from different industries (textile, pharmaceutical, food and others), owing to its

high efficacy for the destruction of a wide range of contaminants in aqueous solutions [17]. The Fenton reaction could be described using the following equations:

$$Fe^{2+} + H_2O_2 \rightarrow Fe^{3+} + OH^{\bullet} + OH^{-} \quad (1)$$

$$Fe^{3+} + H_2O \rightarrow Fe^{2+} + HOO^{\bullet} + H^{+} \quad (2)$$

The process is very efficient in converting organic molecules into less toxic compounds and, in some cases, in their complete mineralization. The Fenton reaction results in the formation of hydroxyl radical ($OH^{\bullet}$), a very powerful oxidant which can initiate the degradation of many organic molecules [18]. However, this radical has a limited life time and is not selective. In contrast, the sulphate radical, $SO_4^{-\bullet}$ (E_0=2.5-3.1 V) [19], due to its high reactivity and stability, allows effective removal of organic compounds present in the environment where $OH^{\bullet}$ failed to achieve efficient degradation. $SO_4^{-\bullet}$ is generated from peroxymonosulfate (PMS) or persulfate precursors through pyrolysis, radiolysis, photolysis or chemical means [20, 21]. Chemical activation is commonly achieved using transition metal ions (Co, Ni, Fe, Mn…) with Co^{2+} being the most effective species [21]. One of the main disadvantages of PMS activation using Co^{2+} in a homogeneous phase is its proven toxicity along with its difficult recovery. Therefore, the last decades have witnessed a growing interest in the preparation of supported Co-based catalysts with the aim to limit of Co ions discharge and, at the same time, achieve high reactivity and recovery of the catalyst [14, 22-26].

In recent years, cobalt sulphides ($CuCo_2S_4$, CoS, Co_3S_4, Co_9S_8, etc) have emerged as an interesting class of materials for different catalytic, photocatalytic and electrocatalytic processes [27]. Despite the high-performance of cobalt sulphides in catalytic processes, their application for PMS activation is scarce. For instance, $CuCo_2S_4$ was successfully applied for PMS activation for bisphenol S oxidation. The sulphide spinel showed higher activity compared to the corresponding oxide [28]. Yin et al. assessed the performance CoS loaded on SBA-15 for the catalytic degradation of phenol using PMS, and found that under optimized

conditions, complete removal can be achieved within 10 min [29]. The enhanced activity was ascribed to the homogeneous distribution of cobalt active sites within the porous matrix. Zhu et al. prepared cobalt sulphide nanocrystals supported on graphene nanosheets (Co_3S_4/GN and CoS/GN) and investigated their ability for PMS activation for bisphenol A (BPA) oxidation. A high BPA degradation efficiency was reached using CoS/GN (100% within 8 min) and 40.64% mineralization [30]. The developed catalyst was stable for up to 3 cycles. Wang et al. synthesized Co_9S_8 and CoO nanostructures encapsulated with nitrogen and sulfur co-doped sludge-derived biochar [31] and nitrogen, sulfur and oxygen co-doped carbon armored cobalt sulfide [32], and applied them successfully for sulfamethoxazole degradation using PMS. Li et al. demonstrated the higher efficiency of CoS_2 as compared to Co_3S_4, and Co_9S_8 hollow nanospheres for PMS activation for ciprofloxacin degradation [33].

In this work, we assessed the efficacy of reduced graphene oxide (rGO) decorated with cobalt sulphide nanoparticles (CoS-rGO) for PMS activation for the removal of organic pollutants, including rhodamine B (RhB) and pentachlorophenol (PCP) in aqueous media. Upon optimization of operating conditions, the CoS-rGO/PMS system achieved complete degradation of the pollutants in relatively short times with a total organic content (TOC) of 89% for PCP and 95% for RhB.

2. Experimental Section

2.1. Preparation of cobalt sulphide-reduced graphene oxide (CoS-rGO) nanocomposite

The CoS-rGO nanocomposite was synthesized adopting a solvothermal technique, according to a previous procedure [34]. The detailed synthesis is described in the Supporting Information (**SI**) file.

2.2. Catalytic oxidation procedure

The catalytic decomposition was conducted at room temperature in a spectrometric quartz cuvette by adding 0.4 µL of PMS (0.05 mM) to 2 mL of RhB (30 µM) previously prepared in the presence of (0.1, 0.25 or 0.5 g/L) CoS-rGO catalyst. The resulting mixture was maintained under constant stirring to achieve a homogeneous suspension. The course of the RhB degradation was followed by UV–vis spectrophotometry (Bio-UVmc² spectrophotometer Safas, Monaco) in the wavelength range of 250-800 nm at 554 nm.

The decomposition efficacy was determined using the equation (3):

$$Degradation(\%) = \frac{(C_0 - C)}{C_0} \times 100 = \frac{(A_0 - A)}{A_0} \times 100 \qquad (3)$$

where C_0 and C correspond respectively to the initial and final concentrations of RhB, and A_0 and A stand respectively for the initial and final absorbance of RhB at 554 nm.

The stability of CoS-rGO for the degradation of RhB was evaluated through recycling experiments as follows: a mixture of RhB (30 µM), CoS-rGO (0.25 g/L) and 0.4 µL of PMS (0.05 mM) was allowed to react for 8 min (one run). After that, 0.6 µL of a fresh solution of 0.1 M of RhB was added to maintain an initial concentration of 30 µM. This cycle was repeated 8 times.

Similarly, the catalytic decomposition of pentachlorophenol (PCP) using CoS-rGO/PMS was carried out in a quartz cuvette using 2 mL of PCP (0.4 mM) aqueous solution, rGO-CoS (0.5 g/L) and 2.4 µL of PMS (0.3 mM) under continuous stirring. The course of the reaction was monitored by recording the decay of the PCP absorption maximum at 220 nm.

3. Results and discussion

3.1. Characterization of CoS-rGO

CoS-rGO nanocomposite was prepared using a solvothermal process, according to our previously published procedure [34]. The nanocomposite was analysed using various analytical techniques to establish its structure, morphology and chemical composition.

Fourier-transform infrared spectroscopy (FTIR) is a well-suited technique for the analysis of polar functional groups. The FTIR spectra of graphene oxide (GO), reduced graphene oxide (rGO), cobalt sulphide (CoS) and cobalt sulphide-reduced graphene oxide (CoS-rGO) are displayed in **Figure 1A**. The characteristic peaks in the FTIR spectrum of GO are observed at ~3415 cm^{-1} (O-H vibrations in COOH moieties and/or intercalated water), 2917 cm^{-1} (C-H stretching), 1730 cm^{-1} (carbonyl C=O stretching), 1626 cm^{-1} (C=C stretching in the aromatic domains), 1399 cm^{-1} (O-H bending vibration), 1228 cm^{-1} (C-O vibrations of epoxy), and 1045 cm^{-1} (C-O vibration of alkoxy) [35]. Upon GO reduction using hydrazine (refer to the **SI** for details), the intensity of vibrations related to oxygen functional groups are reduced significantly while the C=C vibration is blue-shifted to 1604 cm^{-1}. These results clearly indicate GO reduction to rGO and restoration of the aromatic network, in accordance with our previous results [36].

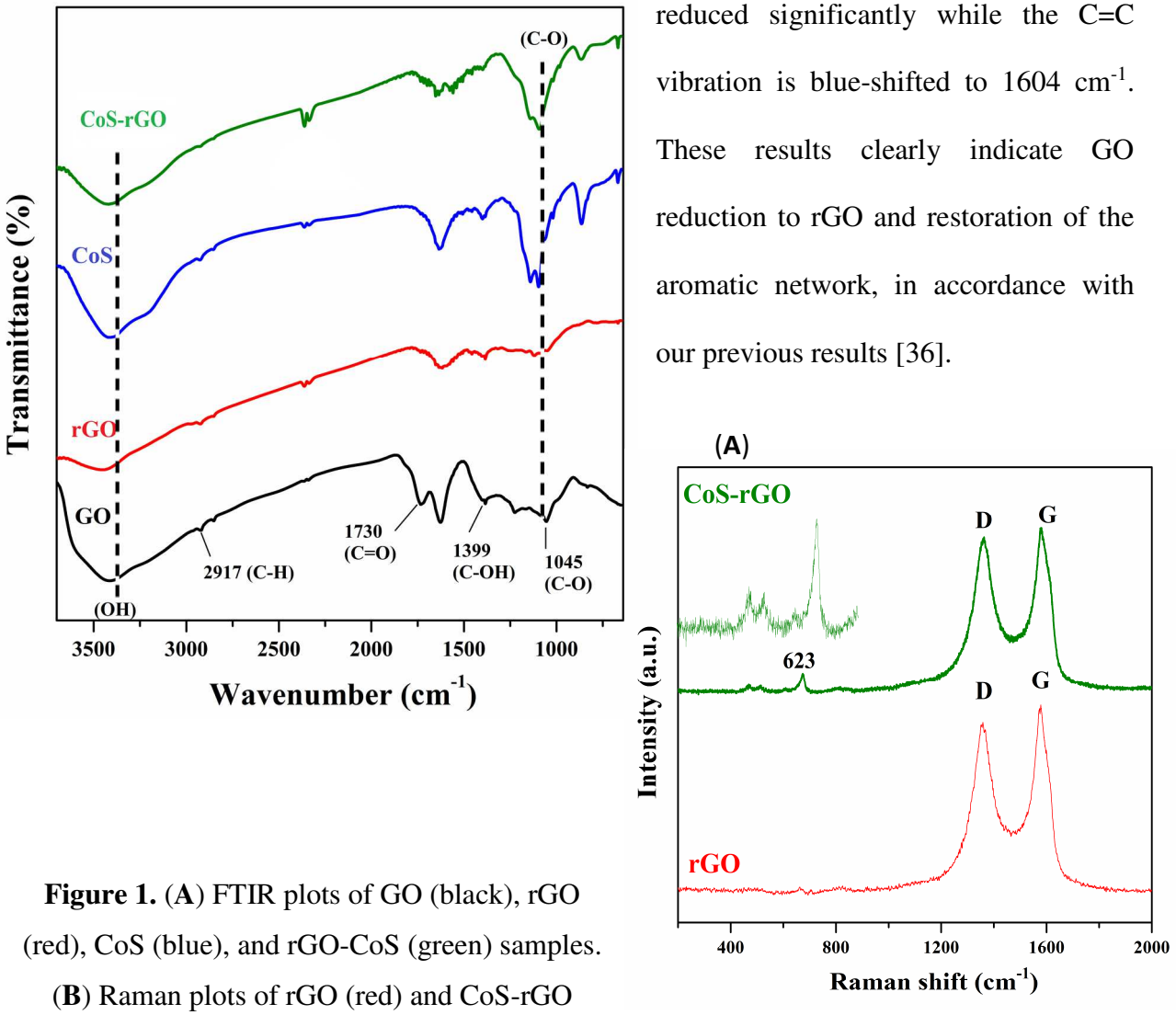

Figure 1. (**A**) FTIR plots of GO (black), rGO (red), CoS (blue), and rGO-CoS (green) samples. (**B**) Raman plots of rGO (red) and CoS-rGO (green). The inset is a zoom in the 300-800 cm^{-1} frequency range.

The FTIR spectrum of CoS comprises several vibration bands at 3412 cm^{-1} (OH stretching), 1629 cm^{-1} (OH bending), 1141 and 1093 cm^{-1} assigned to stretching vibrations of SO_4^{2-} [37]. The 865 and 666 cm^{-1} are attributed to the characteristic stretching vibrations of metal sulphide.[38] Similar vibrations bands were observed in the FTIR spectrum of CoS-rGO with a slight decrease of the vibrations related to H_2O, demonstrating the existence of CoS in CoS-rGO [38].

Raman spectroscopy is a valuable tool for the analysis of carbonaceous materials. **Figure 1B** presents the Raman features of rGO and CoS-rGO. The Raman plot of rGO comprises the characteristic D- and G-bands at about 1340 and 1590 cm^{-1}. The D-band, commonly caused by disordered structure of graphene, is assigned to the breathing modes of sp^2 atoms in rings, while the G-band is ascribed sp^2 atoms stretching in both rings and chains [36]. The Raman spectrum of CoS-rGO consists of the characteristics D- and G-bands of rGO along with small peaks at 410, 495 and 623 cm^{-1} due to CoS. The obvious feature at 623 cm^{-1} is ascribed to ~~stretching vibration~~ A1 mode and the small bands at 410 and 495 cm^{-1} are related respectively to the E_g and F_{2g} modes of CoS, further proving the existence CoS in the composite [30, 39]. The I_D/I_G ratio is commonly used to assess the amount of defects in graphenic-based materials. The results from the **Table S1** reveal that the I_D/I_G ratio values of rGO (0.86) and CoS-rGO (0.85) are comparable, indicating that the defect content was not affected upon CoS-rGO formation.

The thermal behaviour of the prepared materials was assessed by thermogravimetric analysis (TGA), **Figure S1**. The thermogram of rGO comprises three different weight loss stages. The first one (18 wt.%) below 100°C was most likely due to water evaporation. This was followed by another 31 wt.% loss in the 100-250°C temperature range ascribed to the evaporation of organic-containing oxygen groups. Thereafter, a steady weight loss was registered to reach about 75 wt.% at 900°C. The thermal degradation of bare CoS comprised

several stages: about 7 wt.% loss between room temperature and 150°C ascribed to adsorbed water evaporation, 15 wt.% loss in the 150-250°C temperature range attributed to evaporation of reagent residues; the weight loss recorded above 250°C was assigned to CoS sublimation with a residual mass of 40% at 900°C [40]. The thermogram of CoS-rGO follows the same trend as that of CoS with residual mass of about 23% at 900°C.

The chemical composition of CoS-rGO sample was analysed by X-ray photoelectron spectroscopy (XPS). The XPS wide scan in **Figure S2a** comprises the main characteristic elements i.e. C, O, S and Co [34]. The atomic percentages of Co and S, determined from the survey spectrum, are respectively at 20.60 and 7.33 at.%. The Co/S ratio is 2.81, indicating a deviation from the stoichiometric composition of the material and the presence of other Co phases.

The high-resolution spectrum of the C_{1s} can be deconvoluted into three peaks at ~284.3, 286.0 and 287.7 eV due respectively to graphitic sp^2 (C-C), C-O and C=O species (**Fig.S2b**). The core level spectrum of the Co_{2p} (**Fig. S2c**) is curve-fitted with several bands at 780.9 and 796.8 eV with a spin orbit split of 15.9 eV due to Co^{2+} in CoS [41]. The bands at 784.8 and 801.8 eV are ascribed to Co^{2+} in $CoSO_4$; the satellite peaks at 789.3 and 801.8 eV are characteristic of Co^{2+} [34]. The core level plot of the S_{2p} (**Fig. S2d**) consists of two main bands at around 162 and 168 eV due respectively to S_{2p} in CoS and $CoSO_4$. Both bands are fitted with peaks due to $S_{2p1/2}$ and $S_{2p3/2}$ at respectively 161.5 and 163.4 eV for CoS and 167.5 and 170.2 eV for $CoSO_4$.

TEM and HAADF-STEM images of the CoS-rGO are depicted in **Figure S3**. **Figure S3a** shows plenty of CoS nanoparticles homogeneously anchored on the sheets of rGO. TEM images (**Fig. S3b-d**) suggest that, during the synthesis, the CoS particles underwent agglomeration. The elemental mapping of different elements confirmed a good homogeneous distribution of the carbon, oxygen, cobalt and sulphur elements.

3.2. Catalytic decomposition of pollutant molecules

3.2.1. Rhodamine b (RhB) degradation using CoS-rGO/PMS

The catalytic efficacy of CoS-rGO was examined for RhB (model pollutant) decomposition in presence of potassium peroxymonosulfate (PMS). In **Figure 2** are displayed the absorption spectra of a mixtutr of RhB (30 µM) and CoS-rGO (0.25 $g.L^{-1}$) before and after addition of PMS (0.05 mM).

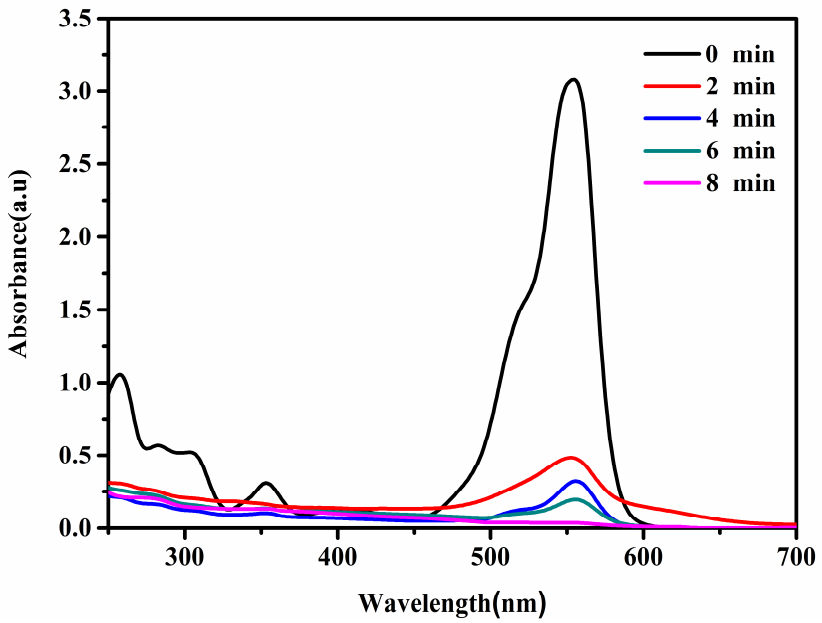

Figure 2. The absorption spectra of a mixture of RhB (30 µM) and CoS-rGO NPs (0.25 g/L) before and after PMS (0.05 mM) addition at room temperature.

A fast decrease of the absorption features and particularly the peak at λ_{max}=554 nm was observed over time. Interestingly, there is no apparent shift in the absorption peak with a complete decomposition after 8 min reaction.

To shed light on the synergistic effect of CoS and rGO, several control experiments were carried out (**Fig. S4**). PMS (0.05 mM) alone, in absence of CoS-rGO, was not efficient for RhB degradation under our operating conditions. Similarly, in absence of PMS, rGO, CoS or CoS-rGO achieved limited RhB removal (<10% maximum observed for CoS-rGO), due most

likely to RhB adsorption on the catalysts' surface. From these results, we can conclude that RhB was stable in presence of PMS and CoS-rGO taken separately. Additionally, rGO alone was not efficient for PMS activation with about 10% degradation after 16 min. The result contrasts with the performance achieved by CoS. Indeed, CoS (0.25 g/L) was able to induce complete RhB (30 µM) decomposition in presence of PMS (0.05 mM) after 10 min.

3.2.2. Effects of initial RhB concentration, PMS loading, CoS-rGO loading, pH, and temperature

Several operating parameters like PMS concentration, CoS-rGO loading, pH, and solution temperature, that may influence the RhB degradation were systematically investigated (**Fig. 3** and **Fig.S5**).

The influence of initial RhB concentration was studied using CoS-rGO loading of 0.25 g/L and PMS concentration of 0.05 mM. As can be observed in **Figure S5**, by elevating the initial RhB concentration from 30 to 50 µM, the degradation time increased from 8 to 18 min. This could be due to the low concentration of $SO_4^{-\bullet}$ and $OH^{\bullet}$ radicals produced under these experimental conditions to compensate the increase of the RhB concentration.

Figure 3a presents the RhB (30 µM) degradation process using various PMS concentrations (0.01, 0.05, and 0.1 mM) in presence of CoS-rGO (0.25 g/L). The results revealed a clear dependence of the catalytic process on the PMS concentration at fixed RhB and CoS-rGO concentrations. A complete RhB removal was achieved using 0.1 and 0.05 mM of PMS after 6 and 8 min, respectively. Even though 0.1 mM PMS achieved full degradation of RhB in a shorter time, we selected the lower PMS concentration of 0.05 mM throughout the study.

In the next step, the influence of CoS-rGO catalyst loading on RhB (30 µM) decomposition was assessed using 0.05 mM of PMS (**Fig. 3b**). Here again, the catalytic process was accelerated upon increasing the catalyst loading from 0.1 to 0.5 g/L although

there was no marked difference between 0.25 and 0.5 g/L under our experimental conditions. Thus, a catalyst loading of 0.25 g/L was selected for this catalytic transformation. Based on these results and with the aim to limit the catalyst loading and PMS concentration, the following conditions were applied throughout the study: [CoS-rGO]=0.25 g/L and [PMS]=0.05 mM.

The effect of the initial pH value on RhB decomposition was studied in the pH window between 3 and 10 using RhB (30 µM), PMS (0.05 mM), and CoS-rGO (0.25 g/L). The results in **Figure 3c** revealed that, while the degradation process was slightly affected by the change of the pH of the medium at the initial stage, the full RhB was removal complete after 8 min independent of the pH value of the solution.

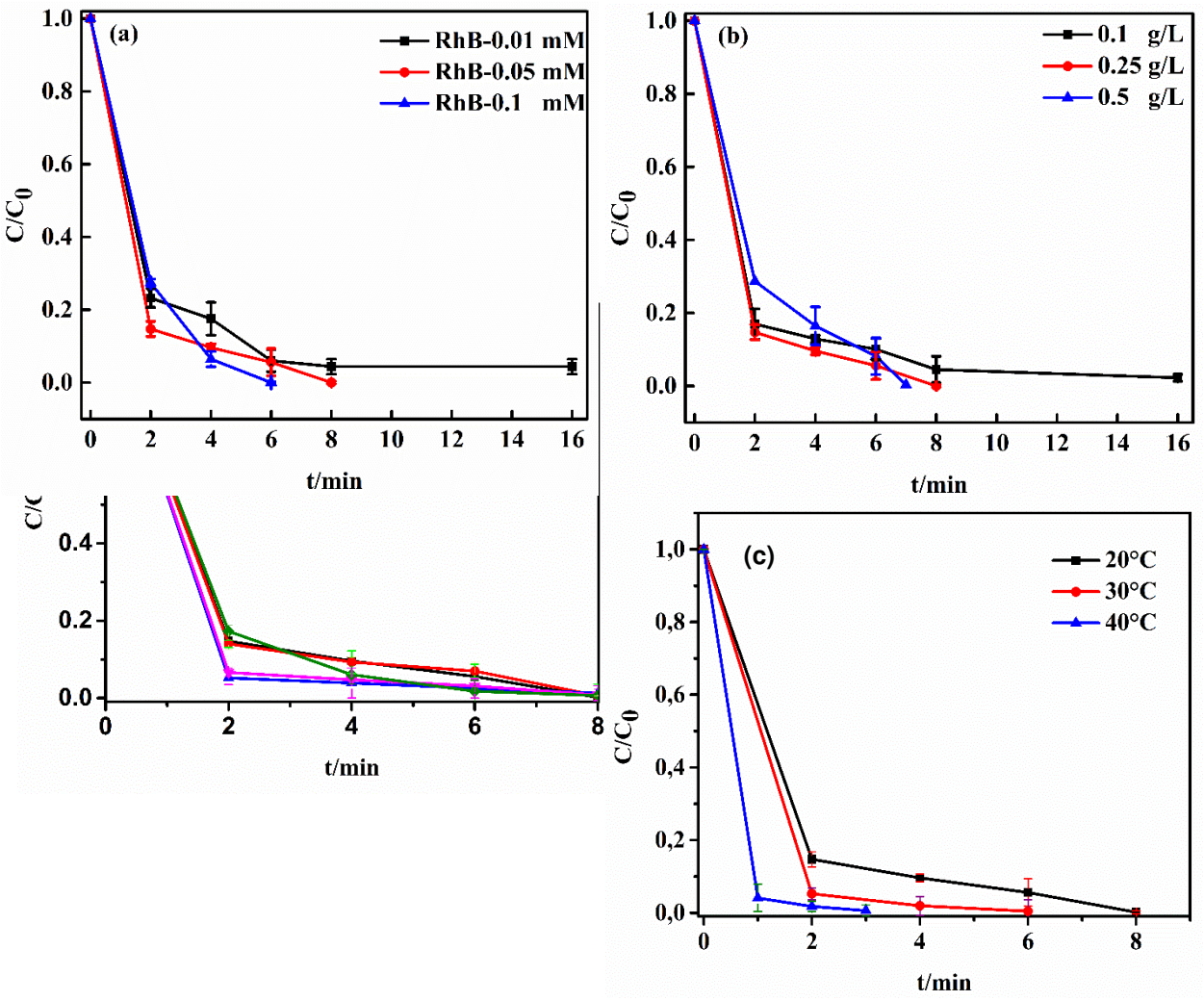

Figure 3. Influence of various operating parameters on RhB removal: (**a**) PMS loading ([RhB]=30 µM, [CoS-rGO]=0.25g/L); (**b**) CoS-rGO catalyst loading ([RhB]=30 µM, [PMS]=0.05 mM); (**c**) pH ([RhB]=30 µM, [PMS]=0.05 mM, [CoS-rGO]=0.25 g/L); (**d**) temperature ([RhB]=30 µM, [PMS]=0.05 mM, [CoS-rGO]=0.25 g/L).

Reaction temperature is another significant parameter affecting PMS activation and consequently the RhB removal process. Therefore, the catalytic decomposition of RhB (30 µM) using PMS (0.05 mM) and CoS-rGO (0.25 g/L) was carried out at 20, 30 and 40 °C. As illustrated in **Figure 3d**, the fastest removal efficiency of RhB was obtained at 40 °C. The kinetics of RhB removal were significantly improved from 0.6714 to 1.7259 min^{-1} upon varying the temperature from 20 to 40 °C.

In terms of reaction kinetics, the entire process could not be described by a zero-order or even a pseudo-first order models. Thus, the first step i.e. the first 4 min of the reaction and the second step (remaining catalytic process) were both fitted with pseudo-first order kinetics using equation (4) [42]:

$$\ln C_t/C_0 = kt + y \qquad (4)$$

where, k the apparent rate constant (min^{-1}), t the reaction time (minutes), y a constant, and C_0 et C_t are respectively the RhB concentration at time t = 0 and t > 0.

For each reaction, two rate constant values (k_1 for the initial stage and k_2 for the remaining degradation process) were determined from the slopes of the two linear curves of the ln C_t/C_0 *vs.* time plots along with the corresponding correlation coefficients (R). The results are summarized in **Table 1**. The k_1, recorded in the first 4 min, gives more information on the initial reaction rate, while the k_2 provides information on the equilibrium between the reactants and the reaction products [42].

The apparent rate constant exhibits a non-uniform variation with the amount of the catalyst, whereas the variation is more uniform with the increase in PMS loading. During the first 4

min of the catalytic process, RhB degradation rate constant is reduced as the catalyst loading increases from 0.1 to 0.5 g/L. For the lowest catalyst concentration tested (0.1 g/L), the RhB removel starts more slowly than for 0.25 g/L, this significant increase in rate constant is also observed at the end of the catalytic process, because of the low content of Co(II) species available at the beginning of the reaction.

Table 1. Kinetic constants k_1 and k_2 according to the kinetics of the first order.

Catalyst dosage (g/L)	PMS concentration (mM)	Rate constant $\mathbf{k_1}$ (min^{-1})	R^2	Rate constant $\mathbf{k_2}$ (min^{-1})	R^2
0.25	0.05	0.67	0.9301	0.65	0.924
0.25	0.1	0.68	0.9942	0.85	0.975
0.25	0.01	0.40	0.9110	0.23	0.813
0.5	0.05	0.48	0.9708	0.62	0.863
0.1	0.05	0.58	0.9069	0.27	0.911

At the end of the catalytic process, the degradation rate constant of RhB for a catalyst loading of 0.1 g/L is lower than that of 0.25 g/L, this can be explained by Co(II) active species consumption [42].

The apparent rate constant for the initiation of the degradation process was found to be uniform and proportional to the PMS concentration. The rate of initiation increased from 0.4 to 0.68 min^{-1} upon increasing the PMS concentration from 0.01 to 0.1 mM. For the remaining time degradation process, the value of k increases with the concentration of PMS.

Therefore, the removal efficiency is obviously ascribed to active sites' availability on the catalyst surface for the reaction with PMS to generate more sulphate radicals ($SO_4^{-\bullet}$). It is clear that upon increasing the cobalt active species, $SO_4^{-\bullet}$ could be generated more rapidly,

which can accelerate the degradation process of the pollutants. The degradation reaction can be described by the following equations (5-8) [42]:

$$\mathrm{rGO-Co(II)S + HSO_5^- \rightarrow rGO-Co(III)S + SO_4^{-\bullet} + OH^-} \quad (5)$$

$$\mathrm{SO_4^{-\bullet} + OH^- \rightarrow SO_4^{2-} + OH^\bullet} \quad (6)$$

$$\mathrm{Co(III)S + HSO_5^- \rightarrow Co(II)S + SO_5^{-\bullet} + H^+} \quad (7)$$

$$\mathrm{SO_4^{-\bullet}/OH^\bullet + RhB\ or\ PCP \rightarrow reaction\ intermediates \rightarrow CO_2 + H_2O} \quad (8)$$

Co(II) regeneration from Co(III) by HSO_5^- (Eq. 7) is an important step that allows a continuity of the reaction and to maintain the presence of Co(II). In addition, the hydroxyl radical ($OH^\bullet$) can be generated (Eq. 6) and can participate in the degradation process.

The performance of CoS-rGO/PMS for RhB degradation was comparable to and even better than that achieved by different catalytic systems described in the recent literature (**Table S2**), with several benefits such the use of low PMS concentration, fast reaction kinetics, and improved stability of catalyst.

3.2.3. Influence of coexisting anions in the water matrix

The presence of anions in the matrix water could affect the performance of the catalytic process. Indeed, it has been reported that the addition of anions can potentially lead to scavenging effects in AOPs [43]. Therefore, the influence of anions (CO_3^{2-}, NO_3^-, Cl^-, SO_4^{2-}, PO_4^{3-} and humic acid), usually occurring in wastewater, on the degradation process was evaluated under optimized conditions i.e. RhB (30 µM), PMS (0.05 mM), and CoS-rGO (0.25 g/L). As seen in (**Fig. S6**), the presence of anions (20 mM) or humic acid (5 mg/mL) in the reaction medium had no effect on the removal kinetics of RhB under our experimental conditions.

3.2.4. Identification of reaction intermediates

To better understand the decomposition process, the course of the catalytic reaction was monitored by high-performance liquid chromatography, HPLC (**Fig. 4a**). The peak of RhB (retention time=13 min), under our operating conditions, disappeared after 8 min with no obvious new peaks due to reaction intermediates. The data indicates that RhB degradation is rapid and takes place with complete destruction of the aromatic structure.

Furthermore, the efficacy of CoS-rGO/PMS system for RhB mineralization was evaluated using total organic carbon (TOC) measurements (**Fig. 4b**). Interestingly, the amount of residual carbon is 5.35% after 8 min using the CoS-rGO/PMS system, confirming RhB mineralization.

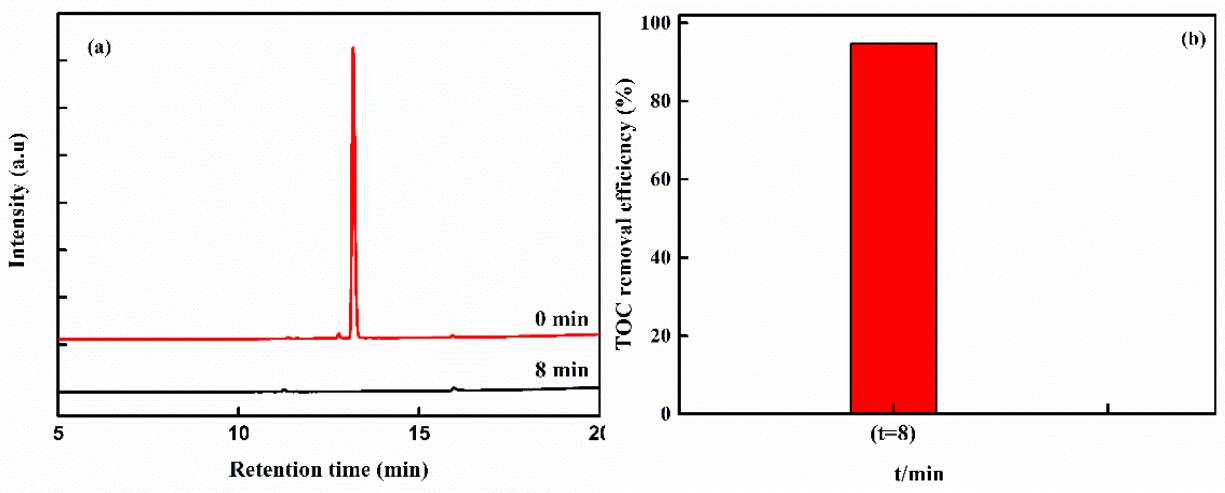

Figure 4. (**a**) HPLC chromatograms of RhB (30 μM) before (black) and after (red) addition of CoS-rGO NPs (0.25 g/L) and PMS (0.05 mM). (**b**) The TOC removal efficiency of RhB.

3.2.7. Stability of CoS-rGO catalyst

To assess the reusability of CoS-rGO, the catalytic degradation of RhB in the presence of PMS over eight cycles was performed using the recycled catalyst (**Fig. 5**). After each cycle, 0.6 μL of a fresh solution of RhB (0.1 M) and 0.4 μL of PMS (0.05 mM) were added to the reaction mixture containing CoS-rGO (0.25 g/L). We found that recycling CoS-rGO did not affect its catalytic efficacy after eight runs, indicating its good stability. Inductively coupled plasma atomic emission spectrometry (ICP-AES) measurement was performed to assess the

amount of cobalt leaching after the cycling stability test. ICP-AES analysis of the supernatant after the 8th cycle revealed the presence of 23.46 µg/L of cobalt, confirming the high stability of CoS-rGO catalyst for RhB degradation by activation of PMS and negligible Co leaching.

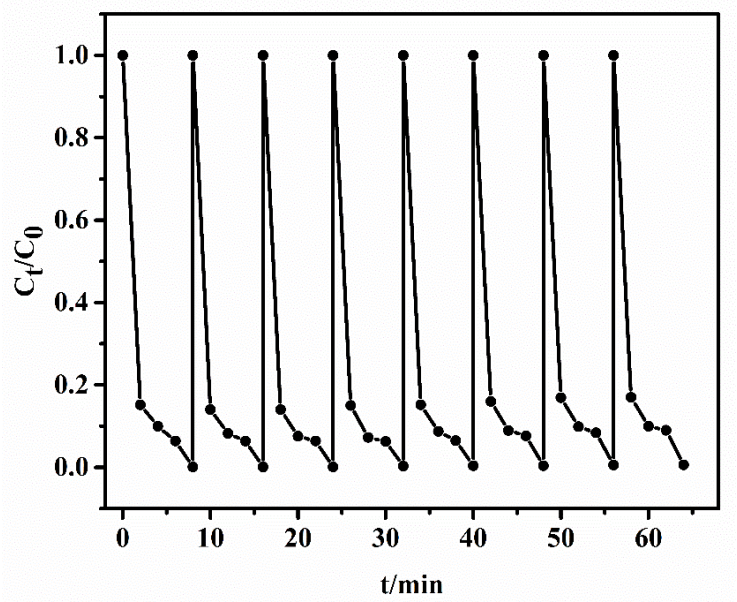

Figure 5. The stability of the CoS-rGO catalyst was studied by recycling experiment of RhB (30 µM) degradation in presence of PMS (0.05 mM) and CoS-rGO (0.25 g/L).

Additionally, zeta potential measurements of CoS-rGO before and after reaction RhB/PMS were recorded to assess any change of the surface charge. The results revealed a slight change of the zeta potential from -14.2±4.3 mV for pristine to -19.2±4.1 mV at the end of the catalytic reaction (**Fig. S7**). This is most likely due to surface oxidation of a small fraction of terminal sulphur atoms of CoS.

To identify the dominant radicals, sulphate ($SO_4^{-\bullet}$) *vs.* hydroxyl ($HO^\bullet$) radicals, formed during PMS activation by the CoS-rGO catalyst, the catalytic removal of RhB by CoS-rGO/PMS was carried out in presence of different scavengers. While ethanol (EtOH) quenches both $SO_4^{-\bullet}$ and $HO^\bullet$ radicals with rate constants of respectively 1.6-7.7×10^7 and 1.2-1.8×10^9 M^{-1}.s^{-1}, *tert*-butanol (TBA) quenches selectively $HO^\bullet$ not $SO_4^{-\bullet}$ radicals [44]. The

scavenging experiment was carried out by addition of EtOH (0.2 M) or TBA (0.2 M) to the reaction mixture of 30 μM of RhB, 0.25 g/L of CoS-rGO and 0.05 mM of PMS. In presence of 0.2 M of TBA, a slight increase of the removal time to 10 min was observed, which contrasts with 18 min recorded upon addition of 0.2 M EtOH (**Fig. 6**). The data suggest that the predominant species in this catalytic process are the sulphate radicals, even though hydroxyl radicals cannot be excluded; the contribution of the latter is minor as compared to that of $SO_4^{-\bullet}$ radicals.

In order to determine whether oxygen species contribute to the degradation process, sodium azide (NaN_3) and *p*-benzoquinone were applied respectively as singlet oxygen (2×10^9 $M^{-1}.s^{-1}$) and superoxide radical anion ($0.1\text{-}1\times10^9$ $M^{-1}.s^{-1}$) scavengers [15]. As can be seen in **Fig. 6**, the degradation reaction was not affected even at high NaN_3 and *p*-benzoquinone concentration of 1 mM, suggesting that the singlet oxygen and superoxide radical anion are not be the primary reactive oxygen species.

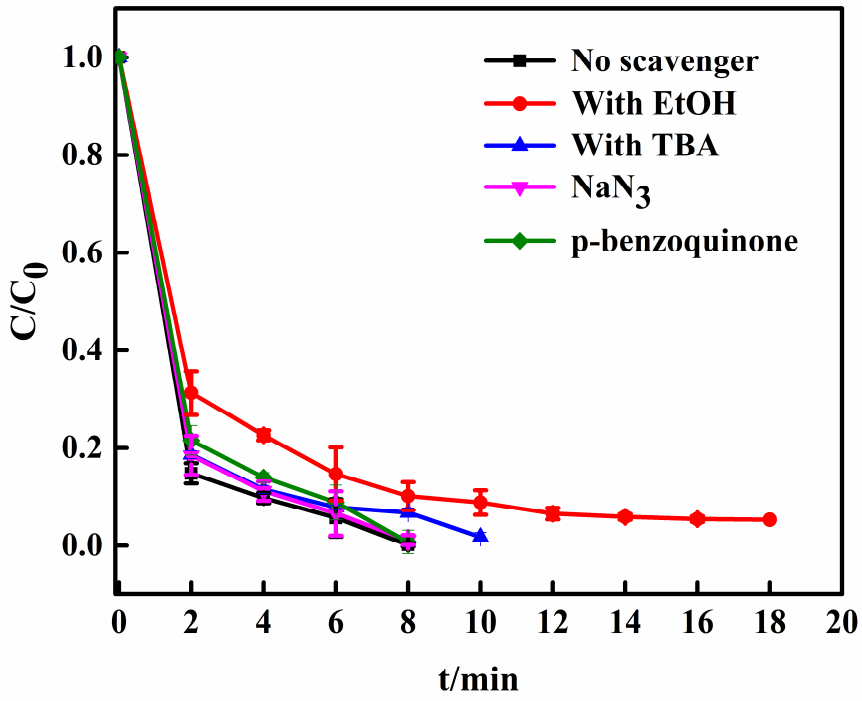

Figure 6. Effect of scavengers ([EtOH]=0.2M, [TBA]=0.2M, [NaN_3]=1mM, [p-benzoquinone]=1 mM) on the removal process of RhB (30 μM) using the CoS-rGO/PMS system.

Additionally, Electron Paramagnetic Resonance (EPR) technique was used to shed light and further validate the presence and contribution of $SO_4^{-\bullet}$ and/or $OH^{\bullet}$ radical species in the RhB removal using CoS-rGO catalyst and PMS oxidant. EPR spectroscopy measurements were carried out at room temperature using DMPO (5,5-dimethyl-1-pyrroline N-oxide) as a spin trap molecule. In absence of CoS-rGO (**Fig. 7A**, pink spectrum), a typical four-peak spectrum of DMPO-$OH^{\bullet}$ spin adduct was observed with its characteristic hyperfine coupling constant A_N=A_H=14.9G, resulting from the PMS hydrolysis, as already reported by Tan et al.[45] However, both DMPO-$OH^{\bullet}$ and DMPO-$SO_4^{-\bullet}$ adducts appeared in PMS and CoS-rGO/PMS systems. The intensity of the signals is much higher in the CoS-rGO/PMS system (**Fig. 7A**, orange spectrum), which denoted that the catalyst improves significantly the radical's formation. Increasing the weight of the catalyst from 0.4 to 1 mg induces slight changes on the EPR spectra.

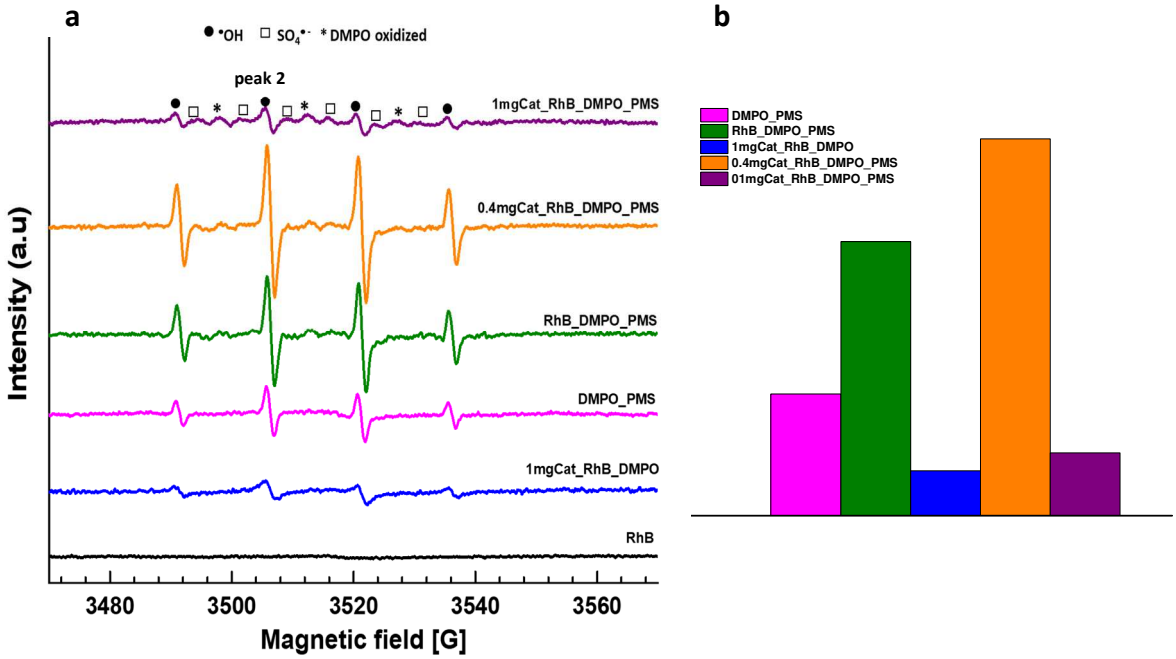

Figure 7. (**A**) EPR spectra of CoS-rGO and CoS-rGO/PMS and rhodamine b. (**B**) double integral of the second peak of DMPO-OH signal. Reactions conditions: [DMPO]=150 mM,

[PMS]=0.45 mM, [RhB]=30 µM. EPR analysis conditions: microwave power: 10.02 mW, amplitude modulation: 1 Gauss.

The amount of $OH^{\bullet}$ species decreases together with an increase of the amount of $SO_4^{-\bullet}$ adduct, as reported in **Figure 7B** (double integral of the second peak of DMPO-$OH^{\bullet}$ signal). This is could be ascribed to $OH^{\bullet}$ species consumption to form $SO_4^{-\bullet}$ radicals, as previously reported by Wang et al. for phenol/PMS/α-MnO_2 system by increasing the time of the reaction [46], according to the following reaction (9):

$$2OH^{\bullet} + 2HSO_5^- \rightarrow 2SO_4^{-\bullet} + 2H_2O + O_2 \qquad (9)$$

3.3. PCP removal using CoS-rGO/PMS system

Encouraged by the high efficacy of the CoS-rGO/PMS system for RhB fast decomposition, we have examined the efficacy of the system for catalytic degradation of pentachlorophenol (PCP), a priority pollutant known for its high toxicity, carcinogenicity, and persistence. PCP degradation using CoS-rGO/PMS system was studied using different operating conditions to find the optimal parameters. The results in **Figure 8** clearly indicate that PCP (400 µM) is stable in presence of CoS-rGO (0.5 g/L) and PMS (0.3 mM), taken separately with less than 10% removal after 20 min. In addition, PCP adsorption on the CoS-rGO surface is negligible under our operating conditions. When the catalytic degradation of PCP (400 µM) was conducted in CoS-rGO (0.5 g/L) and PMS (0.3 mM), a full removal was achieved within 10 min, testifying the efficacy of the CoS-rGO/PMS system for PCP degradation. This contrasts with 68% PCP removal attained after 20 min when the PMS concentration was diminished to 0.1 mM. The process required longer time (20 min) to reach full PCP degradation upon decreasing the PMS concentration to 0.2 mM. The best results were acquired using 0.3 mM PMS and 0.5 g/L of CoS-rGO with an almost full PCP removal (~ 100%) after 10 min.

Other influencing parameters such as catalyst loading (**Fig. S8**), initial PCP concentration (**Fig. S9**), solution pH (**Fig. S10**), and co-existing anions (**Fig. S11**) have been systematically evaluated. When the PCP (400 µM) degradation reaction was carried out using various CoS-rGO catalyst loadings in presence of PMS (0.3 mM), full degradation was observed after 8, 10 and 20 min, respectively for catalyst loadings of 0.75, 0.5, and 0.25 g/L (**Fig. S8**).

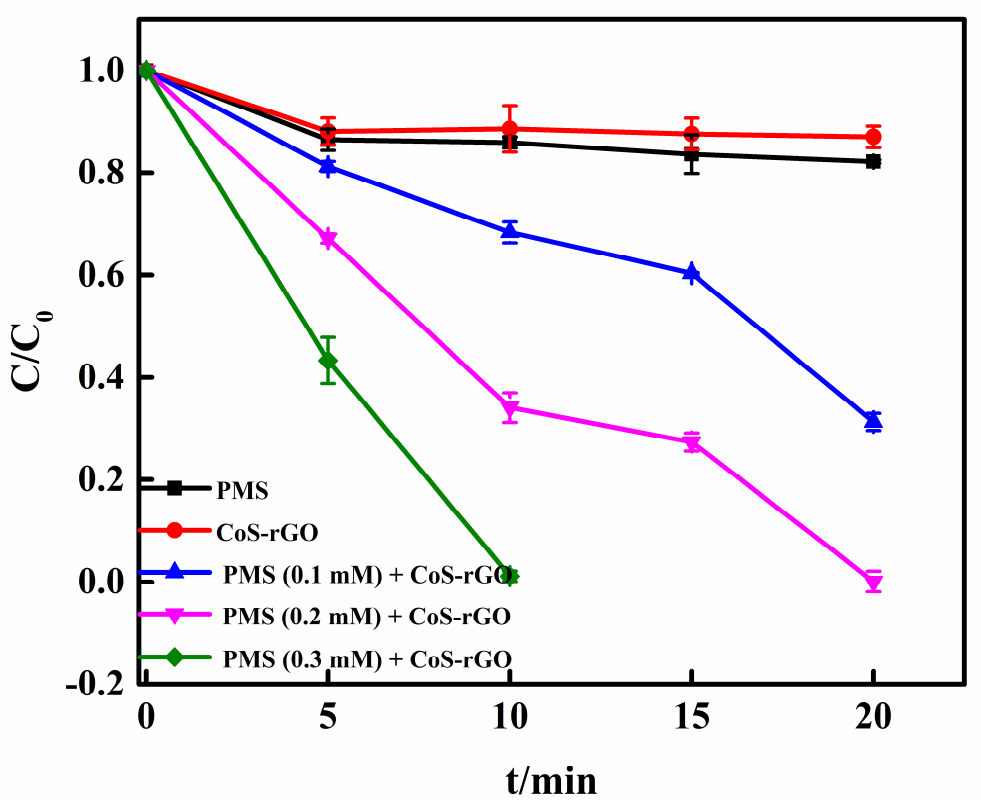

Figure 8. Catalytic degradation of PCP (400 µM) under different operating conditions at room temperature, [CoS-rGO=0.5 g/L].

Consequently, the removal efficiency was obviously ascribed to the availability of active sites for the reaction with PMS to produce sulphate radicals, which can accelerate the PCP degradation. Therefore, a CoS-rGO loading of 0.5 g/L was selected for subsequent experiments. The effect of PCP initial concentration on CoS-rGO/PMS degradation performance was studied in the range of 400 to 600 µM (**Fig. S9**). Obviously, PCP elimination efficiency in the system has decreased upon increasing PCP initial concentration

from 400 to 600 µM. While complete removal was achieved for the lowest PCP concentration investigated i.e. 400 µM within 10 min using 0.5 g/L of CoS-rGO loading and 0.3 mM of PMS, less than 80% PCP degradation was reached after 15 min under otherwise identical experimental conditions for higher PCP concentrations (**Fig. S9**). Hereafter, a concentration of 400 µM of PCP was chosen for further investigations.

The initial dependence of the catalytic degradation was tested by varying the solution pH from 3 to 10 (**Fig. S10**). The impact of pH on the catalytic degradation of PCP is obvious in acid and alkaline conditions with pH=6.4 corresponding to the optimal value at which the highest elimination efficiency and constant rate 0.40519 min^{-1} were achieved. This result could be attributed to many reasons. It is known that the pH of the solution influences the PMS forms; it has been reported in the literature [47] that the pKa_1 of H_2SO_5 is around 0.4 and the pKa_2 is 9.4, which means that the dominant species of PMS at pH 3-7 is HSO_5^-, while HSO_5^- and SO_5^{2-} are the predominant species at a pH of about 9.4. Secondly, PCP elimination was reduced at low pH, because of the stabilizing effect of H^+ on HSO_5^-. It is more difficult to dissociate H from the O-O group of HSO_5^- at acidic pH, which hinders its reaction with catalyst surface and thus PMS activation [48]. Therefore, the maximum removal efficiency was achieved at pH=6.4, testifying that the CoS-rGO/PMS system is suitable for wastewater purification.

Inorganic anions, such as chlorides, sulphates, carbonates, nitrates and phosphates and organic acids (humic acid) are common in water as well as in natural waters, and could potentially react with free radicals and influence the catalytic process. Thus, it is important to study the influence of anions on PCP removal using CoS-rGO/PMS catalytic system. As displayed in **Fig. S11**, the presence of Cl^-, humic acid (HA), CO_3^{2-}, SO_4^{2-} and $H_2PO_4^-$ led to a significant decline of the reaction rate, suggesting that inorganic anions and humic acid have an inhibitory effect. The quenching effect could be ascribed to radical quenching by these

entities. This is due to the structure of pentachlorophenol which is difficult to decompose. The ions added in the solution CO_3^{2-}, NO_3^-, $H_2PO_4^-$ and Cl^- can scavenge (quench) $SO_4^{-\cdot}$ by electron transfer reaction, according to the following reactions (Eqs. 10-13) to form less reactive species to degrade PCP [49].

$$HCO_3^- + SO_4^{-\cdot} \rightarrow HCO_3^{\cdot} + SO_4^{2-} \quad (10)$$

$$H_2PO_4^- + SO_4^{-\cdot} \rightarrow H_2PO_4^{\cdot} + SO_4^{2-} \quad (11)$$

$$NO_3^- + SO_4^{-\cdot} \rightarrow NO_3^{\cdot} + SO_4^{2-} \quad (12)$$

$$Cl^- + SO_4^{-\cdot} \rightarrow Cl^- + SO_4^{2-} \quad (13)$$

CW-EPR measurements were also carried out as in the case of RhB to check the presence and the contribution of $SO_4^{-\bullet}$ and/or $OH^\bullet$ radical species in the PCP degradation by CoS-rGO/PMS system. In the absence of catalyst and organic pollutant (pink spectrum), only $HO^\bullet$ radicals were detected (due to PMS hydrolysis). However, in the presence of both, CoS-rGO catalyst and PCP, two main radicals $OH^\bullet$ and $SO_4^{-\bullet}$ were produced, resulting from the PMS activation by the catalyst. An additional small signal marked by stars was obvious in presence of CoS-rGO, and it could be assigned to an oxidized DMPO, as already reported by Cherifi et al.[50] The increase of the catalyst weight improves significantly the formation of $SO_4^{-\bullet}$ radical whereas the signal of $OH^\bullet$ is diminishing, which indicates that the $SO_4^{-\bullet}$ species originate from $OH^\bullet$ radicals' consumption (**Fig.9b**).

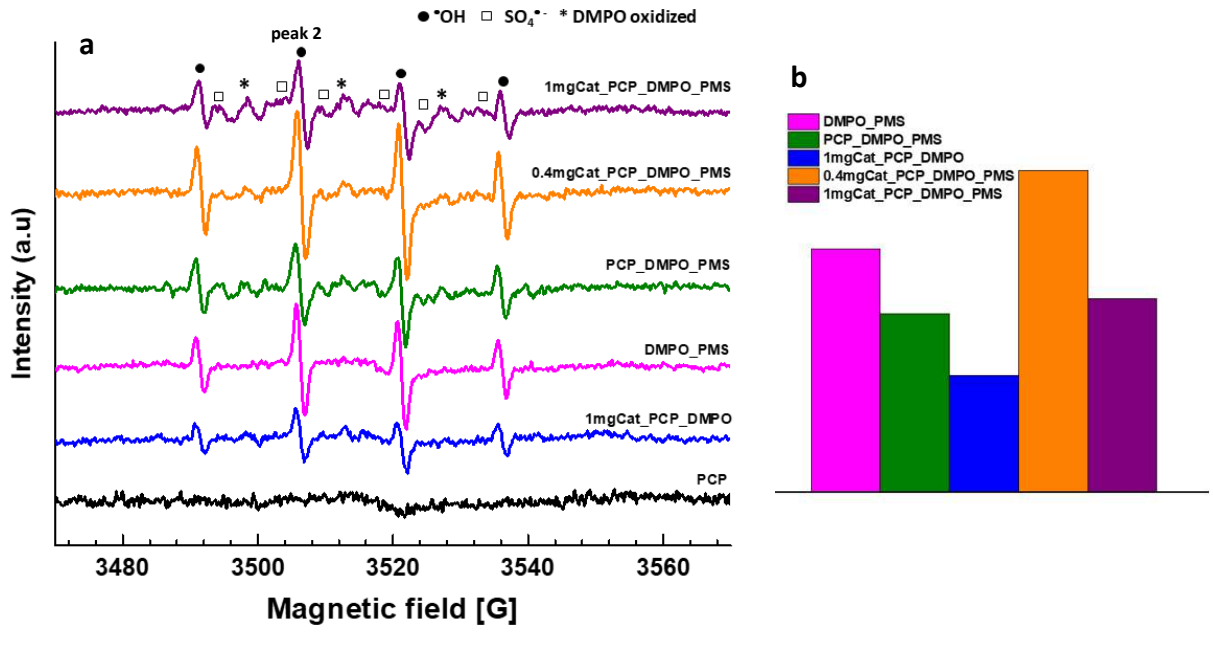

Figure 9. (a) EPR spectra of CoS-rGO and CoS-rGO/PMS and pentachlorophenol. **(b)** double integral of the second peak of DMPO-OH signal. Reaction conditions: [DMPO]=150 mM; [PMS]=0.45 mM; [PCP]=400 µM. EPR analysis conditions: microwave power: 10.02 mW, amplitude modulation: 1 Gauss.

Finally, to gain a better understanding on the PCP catalytic degradation using CoS-rGO/PMS system, HPLC analysis was conducted on the initial PCP solution and after addition of 0.3 mM of PMS and 0.5 g/L of CoS-rGO. **Figure 10a** depicts the chromatogram of the initial PCP aqueous solution, comprising a main peak at around 17 min. The peak completely disappeared 10 min after addition of CoS-rGO/PMS in the PCP solution, confirming the UV-vis analysis. The finding was additionally corroborated by TOC measurements, showing about 89% mineralization of PCP (**Fig. 10b**).

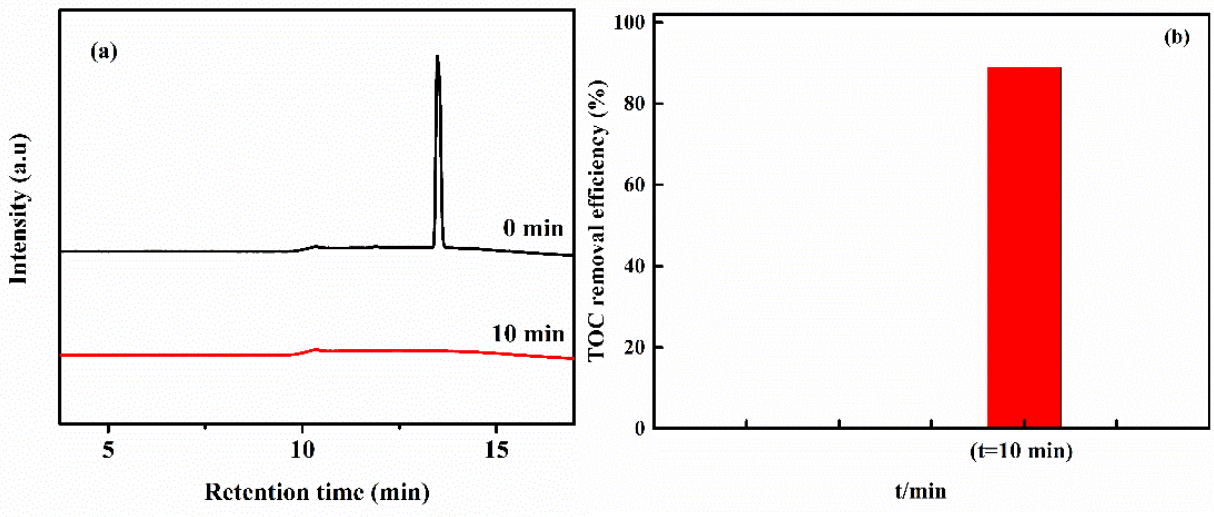

Figure 10. (**a**) HPLC chromatograms of PCP (400 µM) in presence of 0.3 mM of PMS before (black) and after (red) addition of CoS-rGO (0.5 g L^{-1}). (**b**) TOC removal efficiency of PCP.

4. Conclusion

Cobalt sulphide-reduced graphene oxide (CoS-rGO) nanocomposite was prepared using a solvothermal technique and its physico-chemical characteristics were evaluated by FTIR, TGA, Raman, HR-TEM, HAADF-STEM and XPS techniques. The CoS-rGO nanocomposite was applied as an efficient catalyst for PMS activation for the catalytic fast (less than 10 min at room temperature) removal of rhodamine B (RhB) and pentachlorophenol (PCP). Total organic content (TOC) analysis revealed high mineralization efficiency, reaching about 95% and 89% for RhB and PCP, respectively. The catalyst was stable and could be easily reused for eight cycles without apparent activity loss. Quenching experiments along with electron paramagnetic resonance (EPR) measurements revealed that sulphate radicals are the key players in the catalytic process. High stability, enhanced degradation rate, and improved mineralization are some of the benefits of the developed catalyst.

Acknowledgments

The Centre National de la Recherche Scientifique (CNRS), the Hauts-de-France region and the University of Lille are acknowledged for financial support. L.A. thanks the French embassy in Algeria and the Algerian Ministry of Higher Education and Scientific Research (M.E.S.R.S) for a PROFAS B+ 2017 grant.

References

[1] Z. He, S. Yang, Y. Ju, C. Sun, Microwave photocatalytic degradation of Rhodamine B using TiO2 supported on activated carbon: Mechanism implication, J. Environ. Sci., 21 (2009) 268-272.

[2] S. P.Patil, B. Bethi, G. H. Sonawane, V. S. Shrivastava, S. Sonawane, Efficient adsorption and photocatalytic degradation of Rhodamine B dye over Bi_2O_3-bentonite nanocomposites: A kinetic study, J. Ind. Eng. Chem., 34 (2016) 356-363.

[3] I. McLellan, M. Carvalho, C. Silva Pereira, A. Hursthouse, C. Morrison, P. Tatner, I. Martins, M. V. San Romão, M. Leitão, The environmental behaviour of polychlorinated

phenols and its relevance to cork forest ecosystems: a review, J. Environ.l Monitoring, 9 (2007) 1055-1063.

[4] K. Govindan, M. Raja, M. Noel, E. J. James, Degradation of pentachlorophenol by hydroxyl radicals and sulfate radicals using electrochemical activation of peroxomonosulfate, peroxodisulfate and hydrogen peroxide, J. Hazard. Mater., 272 (2014) 42-51.

[5] World Health Organization, Ed., Guidelines for drinking-water quality, World Health Organization, Geneva, 4th ed., 2011.

[6] A. R. Ribeiro, O. C. Nunes, M. F. R. Pereira, A. M. T. Silva, An overview on the advanced oxidation processes applied for the treatment of water pollutants defined in the recently launched Directive 2013/39/EU, Environ. Int. , 75 (2015) 33-51.

[7] J.-G. Yu, X.-H. Zhao, H. Yang, X.-H. Chen, Q. Yang, L.-Y. Yu, J.-H. Jiang, X.-Q. Chen, Aqueous adsorption and removal of organic contaminants by carbon nanotubes, Sci. Total Environ., 482-483 (2014) 241-251.

[8] J. T. Alexander, F. I. Hai, T. M. Al-aboud, Chemical coagulation-based processes for trace organic contaminant removal: Current state and future potential, J. Environ. Management, 111 (2012) 195-207.

[9] R. Muñoz, B. Guieysse, Algal–bacterial processes for the treatment of hazardous contaminants: A review, Water Res., 40, (2006) 2799-2815.

[10] R. T. Gill, M. J. Harbottle, J. W. N. Smith, S. F. Thornton, Electrokinetic-enhanced bioremediation of organic contaminants: A review of processes and environmental applications, Chemosphere, 107 (2014) 31-42.

[11] M. N. Chong, B. Jin, C. W. K. Chow, C. Saint, Recent Developments in Photocatalytic Water Treatment Technology: A Review, Water Res., 44 (2010) 2997-3027.

[12] P. Bautista, A. F. Mohedano, J. A. Casas, J. A. Zazo, J. J. Rodriguez, An overview of the application of Fenton oxidation to industrial wastewaters treatment, J. Chem. Technol. Biotechnol., 83 (2008) 1323-1338.

[13] Y. Luo, W. Guo, H. H. Ngo, L. D. Nghiem, F. I. Hai, J. Zhang, S. Liang, X. C. Wang, A review on the occurrence of micropollutants in the aquatic environment and their fate and removal during wastewater treatment, Sci. Total Environ., 473-474 (2014) 619-641.

[14] A. Mirzaei, Z. Chen, F. Haghighat, L. Yerushalmi, Removal of pharmaceuticals from water by homo/heterogonous Fenton-type processes - A review, Chemosphere, 174 (2017) 665-688.

[15] C. Qi, X. Liu, J. Ma, C. Lin, X. Li, H. Zhang, Activation of peroxymonosulfate by base: Implications for the degradation of organic pollutants, Chemosphere, 151 (2016) 280-288.

[16] J. Herney-Ramirez, M. A. Vicente, L. M. Madeira, Heterogeneous photo-Fenton oxidation with pillared clay-based catalysts for wastewater treatment: A review, Appl. Catal. B, 98 (2010) 10-26.

[17] P. Hu, M. Long, Cobalt-catalyzed sulfate radical-based advanced oxidation: A review on heterogeneous catalysts and applications, Appl. Catal. B, 181 (2016) 103-117.

[18] G. V. Buxton, C. L. Greenstock, W. P. Helman, A. B. Ross, Critical Review of rate constants for reactions of hydrated electrons, hydrogen atoms and hydroxyl radicals (·OH/·O-) in Aqueous Solution J. Phys. Chem. Reference Data, 17 (1988) 513-886.

[19] F. Ghanbari, M. Moradi, Application of peroxymonosulfate and its activation methods for degradation of environmental organic pollutants: Review, Chem. Eng. .J., 310 (2017) 41-62.

[20] W.-D. Oh, Z. Dong, T.-T. Lim, Generation of sulfate radical through heterogeneous catalysis for organic contaminants removal: Current development, challenges and prospects, Appl. Catal. B: Environ., 194 (2016) 169-201.

[21] P. Hu, M. Long, Cobalt-catalyzed sulfate radical-based advanced oxidation: A review on heterogeneous catalysts and applications, Appl. Catal. B: Environ., 181 (2016) 103-117.

[22] J. Wang, S. Wang, Activation of persulfate (PS) and peroxymonosulfate (PMS) and application for the degradation of emerging contaminants, Chem. Eng. J., 334 (2018) 1502-1517.

[23] M.-C. Li, F. Ghanbari, F.-C. Chang, C. Hu, K.-Y. A. Lin, Y. Du, Enhanced degradation of 5-sulfosalicylic acid using peroxymonosulfate activated by ordered porous silica-confined Co_3O_4 prepared via a solventfree confined space strategy, Sep. Purif. Technol., 249 (2020) 116972.

[24] R. Tian, H. Dong, J. Chen, R. Li, Q. Xie, Amorphous Co3O4 nanoparticles-decorated biochar as an efficient activator of peroxymonosulfate for the removal of sulfamethazine in aqueous solution, Sep. Purif. Technol., 250 (2020) 117246.

[25] D. D. Tuan, C. Hung, W. D. Oh, F. Ghanbari, J.-Y. Lin, K.-Y. A. Lin, Porous hexagonal nanoplate cobalt oxide derived from a coordination polymer as an effective catalyst for activating Oxone in water, Chemosphere, 261 (2020) 127552.

[26] D. D. Tuan, W. D. Oh, F. Ghanbari, G. Lisak, S. Tong, K.-Y. A. Lin, Coordination polymer-derived cobalt-embedded and N/S-doped carbon nanosheet with a hexagonal core-shell nanostructure as an efficient catalyst for activation of oxone in water, J. Colloid Interface Sci., 579 (2020) 109-118.

[27] S. Chandrasekaran, L. Yao, L. Deng, C. Bowen, Y. Zhang, S. Chen, Z. Lin, F. Peng, P. Zhang, Recent advances in metal sulfides: from controlled fabrication to electrocatalytic, photocatalytic and photoelectrochemical water splitting and beyond, Chem. Soc. Rev., 48 (2019) 4178-4280.

[28] H. Xu, D. Wang, J. Ma, T. Zhang, X. Lu, Z. Chen, A superior active and stable spinel sulfide for catalytic peroxymonosulfate oxidation of bisphenol S, Appl. Catal. B, 238 (2018) 557-567.

[29] Y. Yin, H. Wu, L. Shi, J. Zhang, X. Xu, H. Zhang, S. Wang, M. Sillanpääd, H. Sun, Quasi single cobalt sites in nanopores for superior catalytic oxidation of organic pollutants, Environ. Sci.: Nano, 5 (2018) 2842-2852.

[30] C. Zhu, F. Liu, C. Ling, H. Jiang, H. Wu, A. Li, Growth of graphene-supported hollow cobalt sulfide nanocrystals via MOF templated ligand exchange as surface-bound radical sinks for highly efficient bisphenol A degradation, Appl. Catal. B, 242 (2019) 238-248.

[31] S. Wang, J. Wang, Peroxymonosulfate activation by Co_9S_8@ S and N co-doped biochar for sulfamethoxazole degradation, Chem. Eng. J., 385 (2020) 123933.

[32] S. Wang, H. Liu, J. Wang, Nitrogen, sulfur and oxygen co-doped carbon-armored Co/Co9S8 rods (Co/ Co_9S_8@N-S-O-C) as efficient activator of peroxymonosulfate for sulfamethoxazole degradation, J. Hazard. Mater., 387 (2020) 121669.

[33] W. Li, S. Li, Y. Tang, X. Yang, W. Zhang, X. Zhang, H. Chai, Y. Huang, Highly efficient activation of peroxymonosulfate by cobalt sulfide hollow nanospheres for fast ciprofloxacin degradation, J. Hazard. Mater., 389 (2020) 121856.

[34] P. Borthakur, G. Darabdhara, M. R. Das, R. Boukherroub, S. Szunerits, Solvothermal synthesis of CoS/reduced porous graphene oxide nanocomposite for selective colorimetric detection of Hg(II) ion in aqueous medium, Sens. Actuators B, 244 (2017) 684-692.

[35] Y. Tadjenant, N. Dokhan, A. Barras, A. Addad, R. Jijie, S. Szunerits, R. Boukherroub, Graphene oxide chemically reduced and functionalized with KOH-PEI for efficient Cr(VI) adsorption and reduction in acidic medium, Chemosphere, 258 (2020) 127316.

[36] M. Budimir, R. Jijie, R. Ye, A. Barras, S. Melinte, A. Silhanek, Z. Markovic, S. Szunerits, R. Boukherroub, Efficient capture and photothermal ablation of planktonic bacteria

and biofilms using reduced graphene oxide-polyethyleneimine flexible nanoheaters, J. Mater. Chem. B, 7 (2019) 2771-2781.

[37] J. Berger, Infrared and Raman Spectra of $CuSO_4$, $5H_2O$; $CuSO_4$, $5D_2O$; And $CuSeO_4$, $5H_2O$, J. Raman Spectros., 5 (1976) 103-114.

[38] S. Ariponnammal, T. Srinivasan, Growth and characterization of cobalt sulphide nanorods, Res. J. Recent. Sci., 2 (2013) 102-105.

[39] S. J. Patil, J. H. Kim, D. W. Lee, Graphene-nanosheet wrapped cobalt sulphide as a binder free hybrid electrode for asymmetric solid-state supercapacitor, J. Power Sources, 342 (2017) 652-665.

[40] A. A. Khan, S. Kumari, A. Chowdhury, S. Hussain, Phase tuned originated dual properties of cobalt sulfide nanostructures as photocatalyst and adsorbent for removal of dye pollutants, ACS Appl. Nano Mater., 1 (2018) 3474−3485.

[41] Y. Chen, S. Xu, S. Zhu, R. J. Jacob, G. Pastel, Y. Wang, Y. Li, J. Dai, F. Chen, H. Xie, B. Liu, Y. Yao, L. G. Salamanca-Riba, M. R. Zachariah, T. Li, L. Hu, Millisecond synthesis of CoS nanoparticles for highly efficient overall water splitting, Nano Res., 12 (2019) 2259-2267.

[42] C. Marinescu, M. Ben Ali, A. Hamdi, Y. Cherifi, A. Barras, Y. Coffinier, S. Somacescu, V. Raditoiu, S. Szunerits, R. Boukherroub, Cobalt phthalocyanine-supported reduced graphene oxide: A highly efficient catalyst for heterogeneous activation of peroxymonosulfate for rhodamine B and pentachlorophenol degradation, Chem. Eng. J., 336 (2018) 465-475.

[43] R. Luo, C. Liu, J. Li, J. Wang, X. Hu, X. Sun, J. Shen, W. Han, L. Wang, Nanostructured CoP: An efficient catalyst for degradation of organic pollutants by activating peroxymonosulfate, J. Hazard. Mater., 329 (2017) 92-101.

[44] S. Dhaka, R. Kumar, M. A. Khan, K.-J. Paeng, M. B. Kurade, S.-J. Kim, B.-H. Jeon, Aqueous phase degradation of methyl paraben using UV-activated persulfate method, Chem. Eng. J., 321 (2017) 11-19.

[45] C. Tan, X. Jian, Y. Dong, X. Lu, X. Liu, H. Xiang, X. Cui, J. Deng, H. Gao, Activation of peroxymonosulfate by a novel EGCE@Fe3O_4 nanocomposite: Free radical reactions and implication for the degradation of sulfadiazine, Chem. Eng. J., 359 (2019) 594-603.

[46] Y. Wang, S. Indrawirawan, X. Duan, H. Sun, H. Ming Ang, M. O.Tadé, S. Wang, New insights into heterogeneous generation and evolution processes of sulfate radicals for phenol degradation over one-dimensional α-MnO_2 nanostructures, Chem. Eng. J., 266 (2015) 12-20.

[47] N. Yang, J. Cui, L. Zhang, W. Xiao, A. N. Alshawabkeh, X. Mao, Iron electrolysis-assisted peroxymonosulfate chemical oxidation for the remediation of chlorophenol-contaminated groundwater, J. Chem. Technol. Biotechnol., 91 (2016) 938-947.

[48] C. Tan, N. Gao, Y. Deng, J. Deng, S. Zhou, J. Li, X. Xin, Radical induced degradation of acetaminophen with Fe_3O_4 magnetic nanoparticles as heterogeneous activator of peroxymonosulfate, J. Hazard. Mater., 276 (2014) 452-460.

[49] S. Khan, X. He, J. A. Khan, H. M. Khan, D. L. Boccelli, D. D. Dionysiou, Kinetics and mechanism of sulfate radical-and hydroxyl radical-induced degradation of highly chlorinated pesticide lindane in UV/peroxymonosulfate system, Chem. Eng. J., 318 (2017) 135-142.

[50] Y. Cherifi, A. Addad, H. Vezin, A. Barras, B. Ouddane, A. Chaouchi, S. Szunerits, R. Boukherroub, PMS activation using reduced graphene oxide under sonication: Efficient metal-free catalytic system for the degradation of rhodamine B, bisphenol A, and tetracycline, Ultrason. Sonochem., 52 (2019) 164-175.

Graphical Abstract